JOURNAL OF THERMOPHYSICS AND HEAT TRANSFER
Vol. 9, No. 2, April–June 1995

Coupled Thermofluid Analysis Method with Application to Thermodynamic Vent Systems

Y. G. Lai,* H. Nguyen,† and J. J. Lee‡
CFD Research Corporation, Huntsville, Alabama 35805

Many practical thermofluid systems involve multiple solid materials and fluid media with vastly differing thermal properties. Thermal and fluid flow analysis in such systems requires a numerical method capable of coupling all participating solid materials and fluid media together. In this article, such a numerical method is presented. The method is based on the multidomain finite volume formulation. Different materials or fluids are represented with different computational domains. A novel implicit coupling procedure at regular and conjugate heat transfer interfaces is designed to obtain the solutions simultaneously and efficiently. The numerical method is first validated against a natural convection between thick-walled eccentric tubes. It is then applied to analyze a zero-*G* thermodynamic vent system. The preliminary three-dimensional analysis results are presented and the thermodynamic characteristics are discussed.

Nomenclature

C = conductivity ratio
C_p = specific heat
G = mass flow over a control volume face
g_i = ith component of the gravity force
J = Jacobian
$\boldsymbol{n}$ = unit normal vector to an interface
P = static pressure
$\boldsymbol{q}$ = heat flow vector through an interface
T = temperature
u_i = ith component of the Cartesian velocity
η = normalized distance
θ = dimensionless temperature
κ = thermal conductivity
μ = molecular viscosity
ρ = density
Φ = viscous dissipation

Introduction

MANY thermofluid systems involve heat exchange between different materials and fluid media. Applications include the thermal management of cryogenic propellant for space missions, cooling of electronic equipments, materials processing, and compact heat exchanger. More often than not, these practical systems have complicated geometries. The thermofluid analysis of such systems requires a numerical method capable of handling complex geometries and coupling all participating materials and fluids together. In this article, a finite volume based numerical method is presented and the above-mentioned requirements are achieved by incorporating the multidomain/multimedia capability. A unique feature of the method is the use of an implicit coupling approach among different domains. In the current formulation the conjugate heat transfer within a single domain is still retained. As a result, the conventional conjugate heat transfer method, such as the approaches of Patankar[1] and Kelkar et al.,[2] is just a special one-domain version of the current method.

Received Jan. 28, 1994; revision received Oct. 14, 1994; accepted for publication Oct. 17, 1994. Copyright © 1994 by the American Institute of Aeronautics and Astronautics, Inc. All rights reserved.

*Senior Engineer. Member AIAA.
†Aerospace Engineer; currently at NASA Marshall Space Flight Center, Huntsville, AL. Member AIAA.
‡Project Engineer.

The developed numerical method will be used to analyze a zero-g thermodynamic vent system (TVS) being developed by NASA Marshall Space Flight Center and Rockwell International to meet the cryogenic propellant management requirements for space missions. This TVS design differs from the state-of-the-art TVS design in that the tank mixer is replaced with a recirculation pump, and the compact heat exchanger is replaced with a simple heat exchanger, mounted on the spray injection manifold. The function of the recirculation pump and spray injection manifold is to recirculate liquid throughout the length of the tank, and thereby destratify both the ullage gas and liquid bulk regardless of liquid orientation and quantity remaining. A detailed description of the design and the system performance characterization can be found in the paper by Fazah et al.[3] It should point out that the TVS design is an ongoing project. This article will concentrate on the development of necessary numerical tools and the buildup of the numerical model for the system. Some preliminary analyses are carried out and the results are reported. NASA Marshall Space Flight Center is currently carrying out the experimental study of the system. A detailed comparison with the measurements is possible only after the data become available.

Presentation of the Numerical Method

Mathematical Formulation

The present study focuses on prediction of combined fluid flow and heat transfer in complex geometries with multiple materials and fluid media. The fluid is assumed to be steady and incompressible for brevity in the following presentation, although the numerical method is applicable to compressible flows. The properties of the fluid are assumed to be constant except body forces due to buoyancy. The mass, momentum, and energy conservation equations can be expressed as

$$(\rho U_i)_{,i} = 0 \tag{1}$$

$$(\rho U_j U_i)_{,j} = -P_{,i} + [\mu(U_{i,j} + U_{j,i})]_{,j} + \rho g_i \tag{2}$$

$$(\rho U_i C_p T)_{,i} = U_i P_{,i} + (\kappa T_{,i})_{,i} + \Phi \tag{3}$$

ρg_i is the buoyancy force. The above governing equations can be expressed in a body-fitted-coordinate system as

$$\frac{\partial}{\partial \xi_k}(J\rho U^k) = 0 \tag{4}$$

$$\frac{\partial}{\partial \xi_k}(J\rho U^k \phi) = \frac{\partial}{\partial \xi_k}\left(\Gamma J g^{jk}\frac{\partial \phi}{\partial \xi_j}\right) + JS_\phi \tag{5}$$

where $U^k = \boldsymbol{V}\cdot\boldsymbol{\varepsilon}^k$ is the contravariant velocity component; $\boldsymbol{\varepsilon}^k = \nabla\xi_k$ is the contravariant base; J is the Jacobian; $g^{jk} = \boldsymbol{\varepsilon}^j\cdot\boldsymbol{\varepsilon}^k$; ϕ stands for the Cartesian velocity components or temperature.

Discretization

The discretization of Eqs. (4) and (5) are carried out using a finite volume approach. First, the solution domain is divided into a finite number of discrete volumes or "cells," where all variables are stored at their geometric centers. The equations are then integrated over the control volumes by using the Gaussian theorem. For example, the integration of the continuity Eq. (4) leads to

$$G_e - G_w + G_n - G_s + G_h - G_l = 0 \tag{6}$$

where the G represent the mass flows over one of the control volume surfaces and w, e, s, n, l, h represent west, east, south, north, low, high faces of the control volume, respectively. For example, $G_e = (J\rho U^l)_e$ is the mass flow through the east face of the control volume.

The discretization of the general convection-diffusion Eq. (5) can be carried out in a similar fashion. The convective term can be discretized as

$$C = C_e - C_w + C_n - C_s + C_h - C_l = G_e\phi_e - G_w\phi_w + G_n\phi_n - G_s\phi_s + G_h\phi_h - G_l\phi_l \tag{7}$$

with ϕ_e, e.g., being the ϕ evaluated at the center of the east face.

The diffusion term can be split into main diffusion ($j = k$) and cross diffusion ($j \neq k$) as

$$D_M^k = \frac{\partial}{J\partial \xi_k}\left(\Gamma J g^{kk}\frac{\partial \phi}{\partial \xi_k}\right), \qquad k = 1, 2, \text{ or } 3 \tag{8}$$

$$D_c^{jk} = \frac{\partial}{J\partial \xi_k}\left(J\Gamma g^{jk}\frac{\partial \phi}{\partial \xi_j}\right), \qquad j \neq k \tag{9}$$

Without loss of generality, $k = 1$ and $j = 2$ are illustrated below. Integration of the D_M^1 term over a control volume leads to

$$\int\int\int D_M^1 J\, d\xi_1\, d\xi_2\, d\xi_3 = \left(\Gamma J g^{11}\frac{\partial \phi}{\partial \xi_1}\right)_e - \left(\Gamma J g^{11}\frac{\partial \phi}{\partial \xi_1}\right)_w \tag{10}$$

By defining

$$D_{\xi_1} = \Gamma J g^{11} \tag{11}$$

we have

$$\int\int\int D_M^1 J\, d\xi_1\, d\xi_2\, d\xi_3 = -(D_{\xi_1}^e + D_{\xi_1}^w)\phi_P + D_{\xi_1}^e\phi_E + D_{\xi_1}^w\phi_W \tag{12}$$

Therefore, the main diffusion coefficient D_ξ needs to be evaluated at the faces of all control volumes. For the cross-diffusion term, the integration of the D_c^{21} term yields:

$$\int\int\int D_c^{21} J\, d\xi_1\, d\xi_2\, d\xi_3 = \left(\Gamma J g^{21}\frac{\partial \phi}{\partial \xi_2}\right)_e - \left(\Gamma J g^{21}\frac{\partial \phi}{\delta \xi_2}\right)_w \tag{13}$$

By defining $D^{21} = (\Gamma/4)Jg^{21}$ and assuming $\phi_{ne} = \frac{1}{4}(\phi_P + \phi_E + \phi_N + \phi_{NE})$, etc., we have

$$\int\int\int D_c^{21} J\, d\xi_1\, d\xi_2\, d\xi_3 = D_e^{21}(\phi_N + \phi_{NE} + \phi_S + \phi_{SE}) - D_w^{21}(\phi_N + \phi_{NW} + \phi_S + \phi_{SW}) \tag{14}$$

With the above discretization process, the discretized ϕ equation at control volume P can be assembled together in a linear equation form as

$$A_P\phi_P = A_W\phi_W + A_E\phi_E + A_S\phi_S + A_N\phi_N + A_L\phi_L + A_H\phi_H + A_{SW}\phi_{SW} + A_{SE}\phi_{SE} + A_{NW}\phi_{NW} + A_{NE}\phi_{NE} + A_{LS}\phi_{LS} + A_{LN}\phi_{LN} + A_{HS}\phi_{HS} + A_{HN}\phi_{HN} + A_{WL}\phi_{WL} + A_{WH}\phi_{WH} + A_{EL}\phi_{EL} + A_{EH}\phi_{EH} + S^\phi \tag{15}$$

As for other issues of the discretization method, such as the special mass flux evaluation procedure for collocated grid arrangement, readers are referred to Refs. 4–6 for more information.

Multidomain/Multimedia Capability

The major goal of this study is to develop a numerical method capable of analyzing combined fluid flow and heat transfer within multiple fluid media and solid materials. To achieve the goal, a multidomain approach is deemed essential. With the traditional multidomain method, the solution domain is divided into a number of smaller and geometrically simple domains. Each domain is solved independently and a mechanism exists to couple all domains together. Such methods can be found in Refs. 7–10. However, most of the previous multidomain approaches consider only single fluid media and are not immediately applicable for the present purpose.

In this study, the traditional multidomain method is extended to have the capability to handle problems with multiple fluid media and multiple solid materials. The starting point is the approach proposed by Lai et al.[10] This approach is chosen due to its distinctive feature of using fully implicit schemes. In the paper by Lai et al.,[10] an implicit zonal interface treatment was demonstrated to be much more efficient compared to the commonly used Schwarz explicit approach. Such efficiency is considered to be essential to resolve the stiffness associated with the conjugate heat transfer problems. A detailed approach was presented in Ref. 10 and will not be repeated here. Only the new features developed for this study are discussed.

With the current extension, the thermofluid problem is divided into a number of smaller domains based on the material difference and geometry complexity. The domain interface could be the natural surface between a fluid and a solid, or an arbitrary cut in the same fluid/material. Each domain is now treated as an independent fluid flow/heat transfer problem. As a result, each domain has its own fluid/material properties, solution control parameters, boundary conditions, etc. This concept is illustrated in Fig. 1a where four domains are used to cover the solution domain of interest. The dashed line represents the interface cut in the same fluid. Since each domain is independent in terms of problem setup, this multidomain concept makes the representation of multiple fluid and multiple solid materials a simple task. To make the solution procedure efficient, however, the final algebraic equations in each block will be assembled together and are solved simultaneously among blocks. It is this implicit solution procedure that makes the current approach distinctive from others.

A further step towards the versatility of the approach is to have unrestricted orientation of three local body-fitted-coordinates within each domain as illustrated in Fig. 1a. This arbitrary orientation of the coordinates will facilitate the grid generation procedure and is unavoidable for many applica-

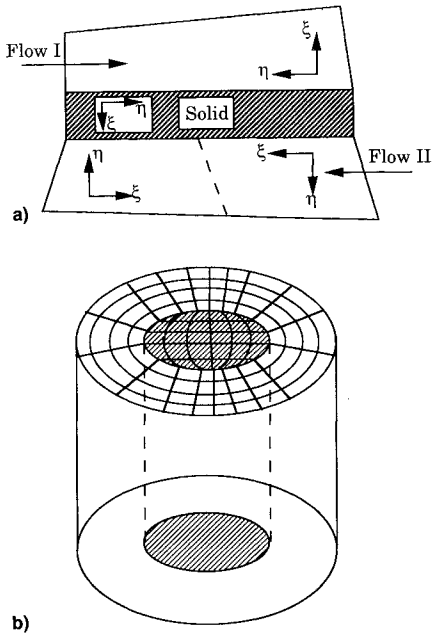

Fig. 1 Schematics of multidomain concept with arbitrary local grid orientation: a) four domains with two fluids and one solid and b) combined H-grid and O-grid.

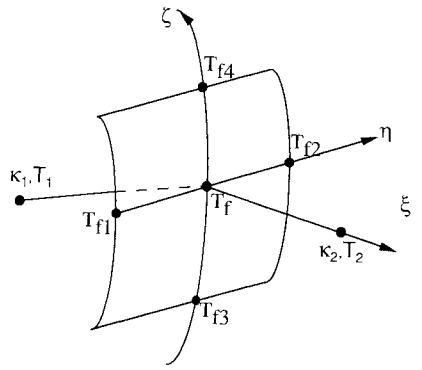

Fig. 2 Illustration for the conjugate heat transfer treatment.

tions. For example, for the flow through a pipe, an H-grid is a better choice than an O-grid since the H-grid eliminates the singular polar point at the center. However, if the conjugate heat transfer analysis between the pipe wall and the fluid is considered, an O-grid is the natural selection for the domain between concentric walls. The H-grid and O-grid combination is illustrated in Fig. 1b and can only be handled using multidomain with arbitrary grid orientation. This kind of H-grid and O-grid combination is extensively used in this study when the TVS system is analyzed later.

Conjugate Heat Transfer Treatment

It is noticed that the domain interface between two different materials/fluids is quite special since the temperature gradient and the material properties are discontinuous there. A special treatment is therefore required at such discontinuous interfaces for a coupled analysis across two media. This is usually known as the conjugate heat transfer problem.

Physical arguments suggest that the temperature and the heat flow across an interface must be continuous. Mathematically, it is written as

$$(T_f)_{\text{Side 1}} = (T_f)_{\text{Side 2}}$$
$$(\boldsymbol{q}_f \boldsymbol{n})_{\text{Side 1}} = (\boldsymbol{q}_f \boldsymbol{n})_{\text{Side 2}} \tag{16}$$

where T_f is the interface temperature, $\boldsymbol{q}_f$ is the heat flow vector, $\boldsymbol{n}$ is the unit normal vector to the interface, and subscripts 1 and 2 represent the materials on the two sides of the interface (see Fig. 2 for the notation). The heat flow vector through an area S can be obtained using Fourier law as

$$\boldsymbol{q} = -\kappa \nabla T S \tag{17}$$

with κ being the thermal conductivity and ∇ being the gradient operator. The above compatibility conditions serve as the starting point for deriving the conjugate heat transfer treatment scheme and the same conditions have been used in Ref. 2.

If the materials on the two sides are the same and the grid line across the interface is continuous, the heat flow through the west–east oriented face can be expressed as

$$-q_f = \left(\kappa \frac{\partial T}{\partial n}\right)_f S_f = A(T_2 - T_1) + B(T_{f2} - T_{f1}) + C(T_{f4} - T_{f3})$$

with

$$A = \kappa(\boldsymbol{\varepsilon}^1 \cdot \boldsymbol{e}^1) S_f, \quad B = \kappa(\boldsymbol{\varepsilon}^2 \cdot \boldsymbol{e}^1) S_f, \quad C = \kappa(\boldsymbol{\varepsilon}^3 \cdot \boldsymbol{e}^1) S_f \tag{18}$$

where $\boldsymbol{\varepsilon}^1$, $\boldsymbol{\varepsilon}^2$, $\boldsymbol{\varepsilon}^3$ are the contravariant base vectors and $\boldsymbol{e}^1$, $\boldsymbol{e}^2$, $\boldsymbol{e}^3$ are the unit contravariant base vectors. In the above, A term is the main diffusion, while B and C terms are the cross diffusion according to the classification presented in the discretization section.

If the materials 1 and 2 are not the same, the compatibility condition (16) can be used. Similar to Ref. 2, a one-sided differencing is used for the main diffusion term $[(\partial T/\partial \xi)$, e.g., in Fig. 3]. With tedious algebraic derivation, one can obtain the interface temperature and heat flux as

$$T_f = \frac{A_1 T_1 + A_2 T_2}{A_1 + A_2} + \frac{(B_2 - B_1)(T_{f2} - T_{f1}) + (C_2 - C_1)(T_{f4} - T_{f3})}{2(A_1 + A_2)} \tag{19}$$

$$-q_f = \frac{2A_1A_2(T_2 - T_1)}{A_1 + A_2} + \frac{(A_1B_2 + A_2B_1)(T_{f2} - T_{f1}) + (A_1C_2 + A_2C_1)(T_{f4} - T_{f3})}{A_1 + A_2} \tag{20}$$

In comparison to Eq. (18), it is clear that the conjugate heat transfer interface can be treated the same way as the single

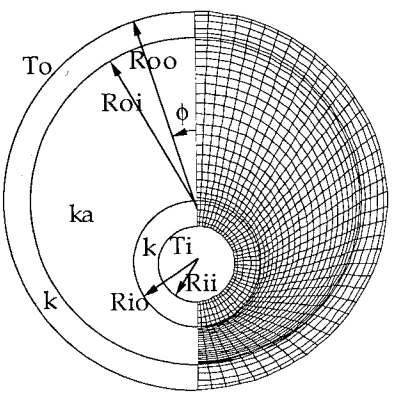

Fig. 3 Geometry and grid used for the natural convection calculation.

media interface. The only difference is to define equivalent diffusion coefficients A, B, and C in Eq. (18) as

$$A_e = \frac{2A_1A_2}{A_1 + A_2}, \quad B_e = \frac{A_1B_2 + A_2B_1}{A_1 + A_2}, \quad C_e = \frac{A_1C_2 + A_2C_1}{A_1 + A_2}$$

With this definition of the equivalent coefficients, the solution of temperature equation can cross the conjugate interfaces continuously and the solution procedure becomes the same as any other dependent variables. In the present study the evaluation of cross term related interface temperatures T_{f1}, T_{f2}, T_{f3}, T_{f4} are different from Ref. 2 and a more accurate approach is used. Firstly, T_{f1}, e.g., is obtained using temperatures of four surrounding cells on both materials 1 and 2. Secondly, the conductivity weighting is used for the averaging since the conventional arithmetic average is still inaccurate if the thermal conductivity on the two sides is vastly different, although it is theoretically second order. It is noted that the above approach does not require continuous grid line across the interface. This feature could simplify the grid generation process for many complex problems. It should also point out that the above formulation is derived based on laminar flows. It is, however, equally applicable to turbulent flows. The only difference is to replace the molecular conductivity with the equivalent turbulent conductivity using a proper wall function.

Validation of the Numerical Method

The above described multidomain conjugate heat transfer method has been applied to many flow and heat transfer problems. In this section, a validation case involving a natural heat convection between thick-walled eccentric tubes is presented. The geometry of the problem is shown in Fig. 3. The inner surface of the inner tube and the outer surface of the outer tube are maintained at two different temperatures, T_i and T_o. The flow is induced by buoyancy forces due to the temperature difference. The Rayleigh number based on the $(T_i - T_o)$ and the length scale of $(R_{oi} - R_{io})$ is taken to be 4.93×10^4, and the Prandtl number for the fluid is 0.7. The same case has been experimentally studied by Kuehn and Goldstein[11] and computationally by Kelkar et al.[2]

A three-domain grid was generated as shown in Fig. 3 with 1271 computational cells (equivalent to 41 × 31 grid). The computation with such a grid takes less than a minute on the Sun Sparc 20 workstation with a seven-order of error reduction in 350 iterations. A finer grid with 5084 cells was also used to study the grid dependence of the results. Such a comparison is shown in Fig. 4a where θ is the dimensionless temperature $(T - T_o)/(T_i - T_o)$, η is the normalized distance between the innermost and the outermost tube walls, and C is the conductivity ratio of the solid and fluid. It was found that the temperature difference is within 5%. Therefore, the 1271-cell grid is deemed adequate for the problem and remaining discussion will use the results from 1271-cell grid. The calculated temperature profiles at $\varphi = 0$ and 180 are displayed in Figs. 4b and 4c, respectively, with four conductivity ratios. The highest C $(=10^4)$ approximates the isothermal tube condition and the results can be directly compared to the experimental study by Kuehn and Goldstein.[11] It is seen that the calculated results are in good agreement with the experimental data. The streamlines and the constant temperature contours of the buoyancy driven flow at two conductivity ratios are shown in Fig. 5.

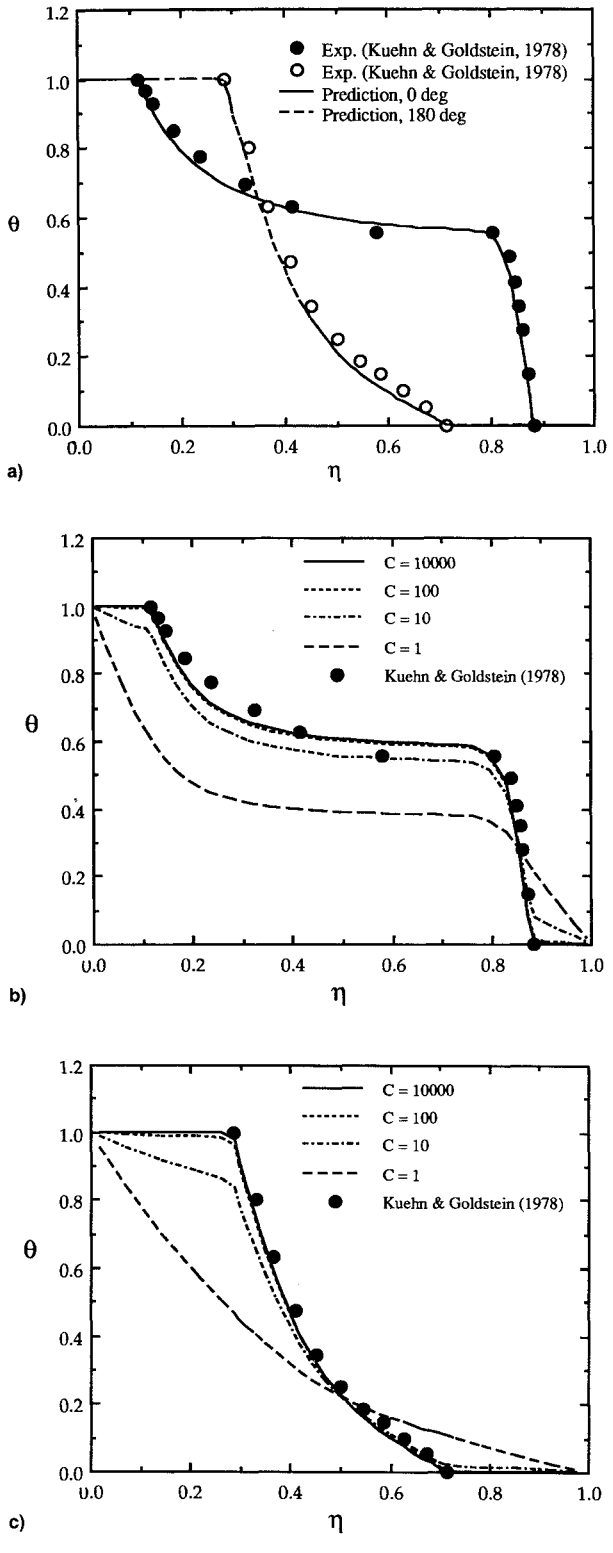

Fig. 4 Comparison between computation and experiment: a) grid independence study, b) along Φ = 0-deg line, and c) along Φ = 180-deg line.

Application to the Thermodynamic Vent System

Brief System Description

In this section, the proposed multidomain/multimedia method is applied to a TVS currently under design and test by NASA Marshall Space Flight Center (MSFC) and Rockwell International. This TVS design is quite innovative in that it integrates the functions of a spray-bar tank mixer and a TVS. This concept not only satisfies the requirement for efficient tank mixing and zero-g venting, but also accommodates thermal conditioning requirements for other components (e.g., engine feed lines, turbopumps, and liquid acquisition devices). The overall design is illustrated in Fig. 6. A more in-depth discussion of the system can be found in Fazah et al.[3] Only the recirculation pump system is the main topic of this computational study.

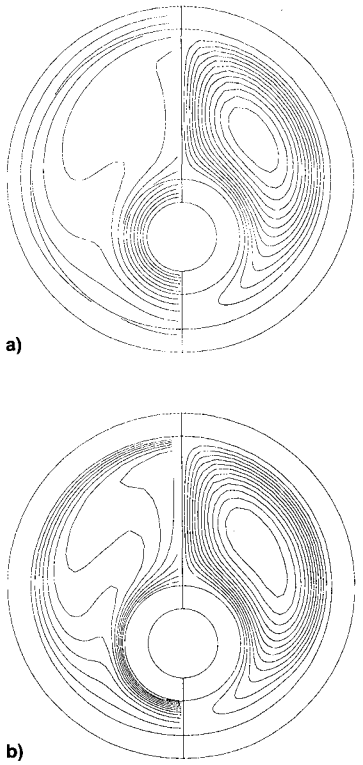

Fig. 5 Temperature and streamline contours at different conductivity ratios. Left: temperature; right: streamlines. C = a) 1 and b) 1000.

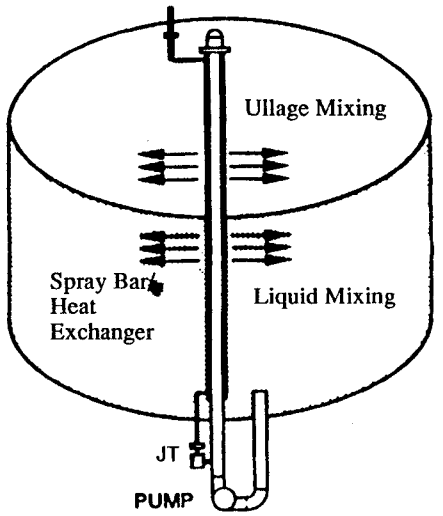

Fig. 6 New TVS design concept.

One cross section view of the preliminary design is shown in Fig. 7a and the U-shaped recirculation system of interest in this study is sketched in Fig. 7b. The recirculation pump system (U-shaped) is installed at the bottom of the LH_2 tank and enclosed by a steel box. The steel box is further insulated using MLI material to prevent heat leakage. In operation, a small amount of LH_2 is allowed to enter the 2-in.-o.d. tube (right branch of the U-tube in Fig. 7b). The flow is later split into two streams: one to a 0.5-in.-o.d. heat exchanger, and another to a 1.5-in.-o.d. tube. The 0.5-in.-diam tube is eventually allowed to expand to a low pressure thereby producing a low heat sink that is used to absorb heat from the LH_2 fluid in the 1.5-in.-diam tube (the heat exchange device is not shown in Fig. 7b).

In this study, the fluid flow and heat transfer process of the recirculation pump system is considered. The operating conditions of the system are assumed to be as follows:

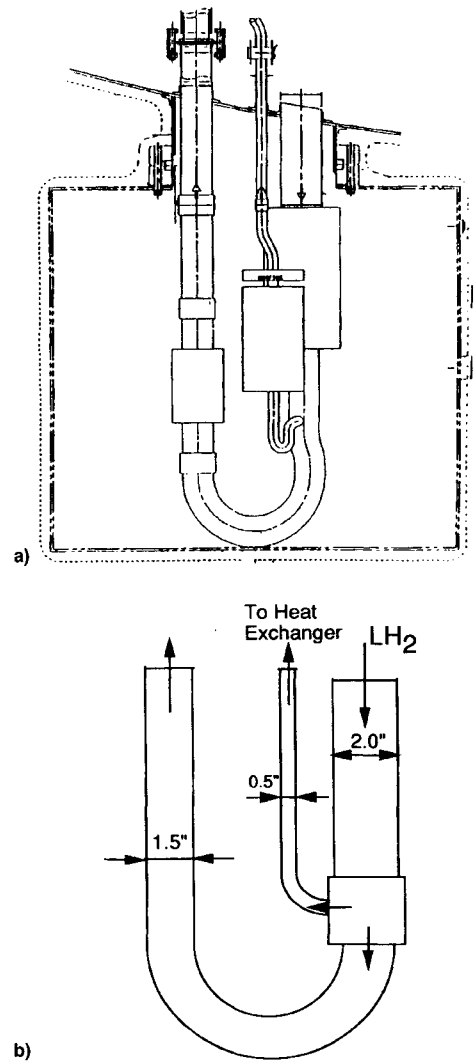

Fig. 7 Cross-sectional view of the recirculation pump system: a) design geometry and b) illustration sketch.

LH_2 mass flow rate:	0.0907 kg/s (0.2 lb/s)
LH_2 inlet temperature:	−252°C
LH_2 inlet pressure:	1.497×10^5 pa
Pump power:	15 W
Ambient temperature:	26°C

Computational Model

The vent system shown in Fig. 7 is numerically represented using a multidomain grid system consisting of 16 domains and involving 36,882 computational cells. Two perspective views of the grid are displayed in Fig. 8. The liquid H_2 flows in the U-shaped tube and in the side heat exchanger are represented by two domains. H-grids are used for the flow domains to avoid the singularity at the center associated with the O-grid. For the same reason, H-grids are used for the central part of the fuel tank bottom and the entire insulation box bottom (see Fig. 8). However, O-grids are used for the rest of the insulation box and for the concentric wall of the U-tubes. These composite grids are made possible due to the multiblock capability and arbitrary coordinate orientation feature discussed before.

The combined fluid flow and heat transfer analysis of this vent system represents a challenging test of the numerical method due to the extreme stiffness of the resultant governing equations. The stiffness of the problem comes from several sources. Firstly, the thermal conductivities for the steel and

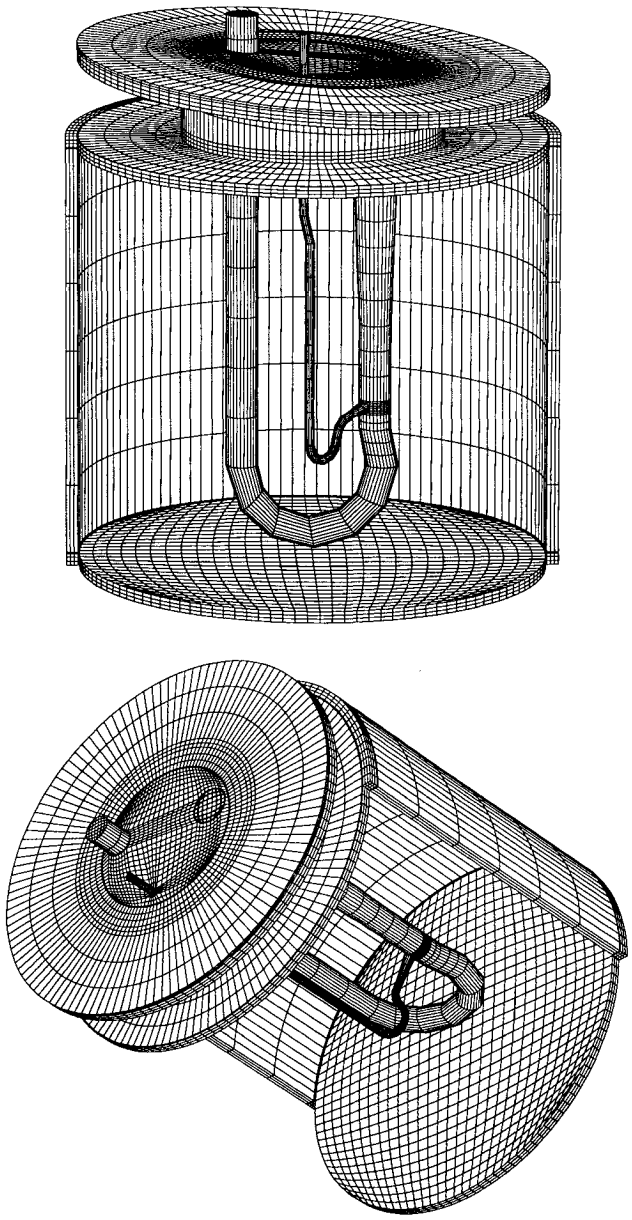

Fig. 8 Two perspective views of the 16-domain grid used for the numerical analysis of the TVS.

the MLI insulation materials are vastly different (15.1 W/m-K for the steel and 5.3×10^{-4} W/m-K for the MLI). Secondly, the insulation layer (MLI) is 10 times thicker than the steel layer. As a result, the final algebraic system has a wide disparity in the eigenvalues and results in a stiff system. In general, an implicit and coupled approach is better able to handle stiff problems.

It is known that the operation of the pump will generate extra heat and be absorbed by the liquid H_2 flow. The amount of heat generation is experimentally determined and treated as a heat source in the numerical model. For the current study, 15-W total heat generation is assumed and this heat source is equally distributed. The boundary conditions of the simulation are specified as follows. The entering liquid H_2 has a flow rate of 0.2 lb/s and fixed temperature of -252°C. The two flow outlets are assumed to be at the same pressure level and fixed pressure boundary conditions are applied at the outlets. Different specification of the exit pressure at the two tube outlets can result in different flow rate through the heat exchanger tube and recirculation tube. Therefore, experimentally determined exit pressures should be provided for a desired design. The space between the recirculation pump system and the insulation box is vacuum, and therefore, all the surfaces inside this space are maintained at adiabatic conditions. A fixed temperature of -252°C is applied to the LH_2 side of the tank bottom plate, the remaining MLI surfaces are treated as either fixed temperature (at 27°C) or fixed heat flux conditions since they are exposed to an ambient environment.

Results and Discussion

Three calculations have been carried out representing three different thermal conditions at MLI out surface. One is the constant temperature (27°C) boundary condition and the other two are the fixed heat flux boundary conditions (at 5 W/m^2 and 10 W/m^2). The heat flux boundary condition is intended to mimic the influence of convective and radiative contribution in the ambient environment.

The calculated results showed that the LH_2 flow in the tubes was seldom affected by the ambient thermal conditions. Due to the large heat capacity of the liquid hydrogen, the LH_2 temperature rises only slightly (~0.004°C) from the inlet to the exits. This suggests that the fluid flow in the recirculation tubes can be assumed isothermal and be analyzed independent of the insulation box.

As mentioned before, the exit pressures at the two tube ends are assumed the same in this calculation. Different exit

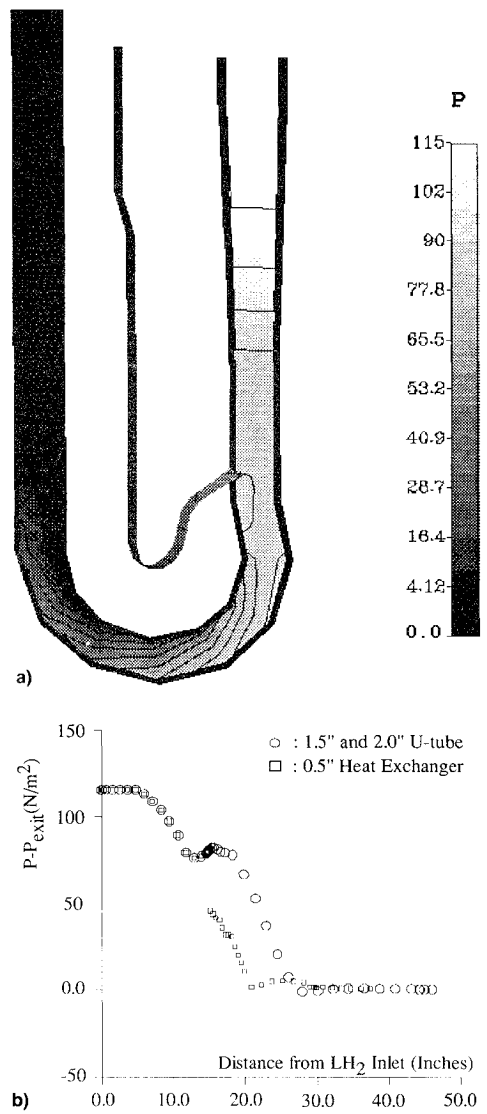

Fig. 9 Pressure distribution in the U-tube and the heat exchanger: a) pressure contours on a cutting plane through the tube center and b) pressure distribution along the tube centerline.

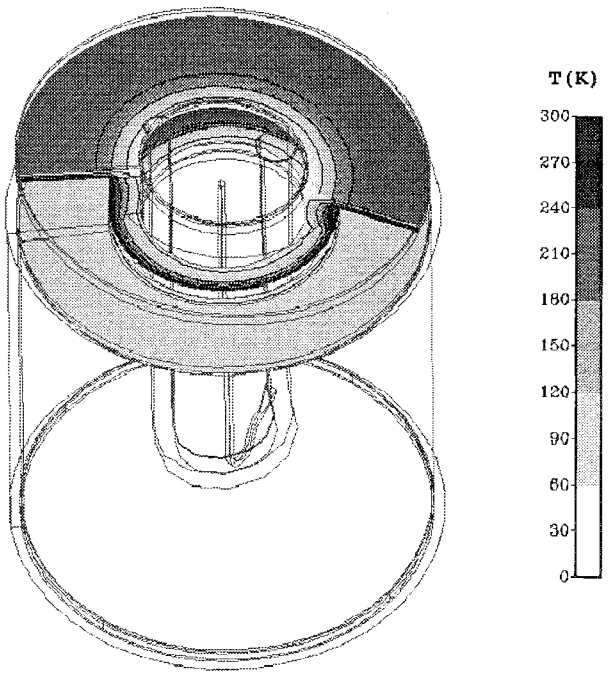

Fig. 10 Temperature contours on several cutting planes.

pressure will lead to different LH_2 flow rate and can be used to achieve the desired flow rate through the heat exchanger tube. The current calculations showed that the LH_2 flow rate through the heat exchanger tube is about 4.4% of the total mass flow rate entering the system. To have a better understanding of the flow system, the pressure distributions in the recirculation pump are displayed in Fig. 9. Figure 9a is the cross-sectional view of the pressure contours and Fig. 9b is the pressure distribution along the centers of the U-tube and the heat exchanger. It is seen that, as expected, most of the pressure loss occurs at the bends and through the pump. The exit pressures of the U-tube and the heat exchanger approach the same values since this is the boundary condition imposed.

From the insulation box, one important quantity is the heat leakage from the environment to the fuel tank. This heat leakage is calculated by evaluating the heat flow rate through the neck part of the recirculation system that is located below the tank bottom. For the three thermal boundary conditions (27°C, 5 and 10 W/m^2) the calculated heat leakage is 6.759, 3.912, and 7.820 W, respectively. Note that the leakage for the 10 W/m^2 case is about twice as much as the leakage for the 5 W/m^2 case. This result is expected since the heat leakage can only go through the ambient environment and the energy has to be balanced. Since the overall solutions are similar for the three cases, only the results from the fixed temperature boundary condition are presented next.

The calculated temperature contours on several cutting planes are shown in Fig. 10. The insulation box is made of two materials: a very thin layer of steel (k = 15.1 W/m-K) and an outside layer of MLI material ($k = 5.33 \times 10^{-4}$ W/m-K). There is a vast difference between the conductivities of the two materials. Therefore, the temperature change mostly occurs inside the MLI and the temperature change in the steel layer is almost negligible. However, it should be pointed out that despite much smaller temperature changes, the steel part is not negligible when the heat leakage is calculated. It is also seen from Fig. 10 that the temperature distribution around the neck portion of the system is quite symmetric despite the inclination of the tank bottom. In view of this, a two-dimensional axisymmetric analysis may provide a good thermal estimation of the system.

Conclusions

A coupled thermofluid analysis method is presented. The numerical method is based on the multidomain (multiblock) finite volume formulation and is capable of handling multiple fluid media and solid materials. A novel implicit coupling procedure at domain interfaces (fluid–fluid, fluid–solid, or solid–solid) is used to enhance the numerical efficiency. Such implicitness is particularly crucial for the fluid–solid or solid–solid type of interfaces where conjugate heat transfer has taken place. The numerical method was implemented into a three-dimensional CFD code that allows the use of a general nonorthogonal grid. The method is first validated by calculating a two-dimensional natural convection problem between thick-walled eccentric tubes. Good agreement is achieved with the available experimental data. Then the numerical method is used to analyze a novel zero-g thermodynamic vent system currently under design by NASA Marshall Space Flight Center and Rockwell International. This analysis is quite preliminary and is intended to demonstrate the usefulness of the numerical method to analyze practical thermodynamic systems.

Acknowledgments

This study is partially supported by NASA Marshall Space Flight Center under Contract NAS8-39812. The authors would like to express their appreciation to James Owen and Van Luoung of NASA-MSFC for participating in several technical discussions, Ashok Singhal and Andrzej Przekwas of CFDRC who provided in-house guidance, and Y. Jiang of CFDRC who participated in the CFD code development.

References

[1]Patankar, S. V., *Numerical Heat Transfer and Fluid Flow*, Hemisphere, Washington, DC, 1980.

[2]Kelkar, K. M., Choudhury, D., and Ambrosi, M., "Numerical Method for the Computation of Conjugate Heat Transfer in Nonorthogonal Boundary-Fitted Coordinates," *Numerical Heat Transfer, Part B*, Vol. 20, 1991, pp. 25–40.

[3]Fazah, M. M., Lak, T., Hguyen, H., and Wood, C. C., "Design and Integrated Operation of an Innovative Thermodynamic Cent System Concept," AIAA Paper 93-2437, June 1993.

[4]Rhie, C. M., and Chow, W. L., "Numerical Study of the Turbulent Flow Past an Isolated Airfoil with Trailing Edge Separation," *AIAA Journal*, Vol. 21, No. 11, 1983, pp. 1526–1532.

[5]Peric, M., Kessler, R., and Schruerer, G., "Comparison of Finite-Volume Numerical Methods with Staggered and Collocated Grids," *Computers and Fluids*, Vol. 16, No. 4, 1988, pp. 389–403.

[6]Lai, Y. G., So, R. M. C., and Przekwas, A. J., "Turbulent Transonic Flow Simulation Using a Pressure-Based Method," *International Journal of Engineering Sciences* (to be published).

[7]Klopfer, G. H., and Molvik, G. A., "Conservative Multizonal Interface Algorithm for the 3D Navier-Stokes Equations," AIAA Paper 91-1601, June 1991.

[8]Rai, M. M., "A Conservative Treatment of Zonal Boundaries for Euler Equations Calculations," *Journal of Computational Physics*, Vol. 62, No. 2, 1986, pp. 472–503.

[9]Benek, J. A., Buning, P. G., and Steger, J. L., "A 3-D Chimera Grid Embedding Technique," AIAA Paper 85-1523, July 1985.

[10]Lai, Y. G., Jiang, Y., and Przekwas, A. J., "An Implicit Multi-Domain Approach for the Solution of Navier-Stokes Equations in Body-Fitted-Coordinate Grids," AIAA Paper 93-0541, Jan. 1993.

[11]Kuehn, J. H., and Goldstein, R. J., "An Experimental Study of Natural Convections Heat Transfer in Concentric and Eccentric Horizontal Cylindrical Annuli," *Journal of Heat Transfer*, Vol. 100, 1978, pp. 635–640.